A&A 607, A37 (2017)
DOI: 10.1051/0004-6361/201731190

Astronomy & Astrophysics

Polarized radiative transfer modeling of warped and clumpy dusty tori

F. Marin[1] and M. Schartmann[2,3,4]

[1] Université de Strasbourg, CNRS, Observatoire astronomique de Strasbourg, UMR 7550, 67000 Strasbourg, France
e-mail: frederic.marin@astro.unistra.fr
[2] Centre for Astrophysics and Supercomputing, Swinburne University of Technology, PO Box 218, Hawthorn, 3122 Victoria, Australia
[3] Universitäts-Sternwarte Muünchen, Scheinerstraße 1, 81679 München, Germany
[4] Max-Planck-Institut für extraterrestrische Physik, Postfach 1312, Giessenbachstr., 85741 Garching, Germany

Received 18 May 2017 / Accepted 21 August 2017

ABSTRACT

Context. Active galactic nuclei (AGN) are anisotropic objects surrounded by an optically thick equatorial medium whose true geometry still defies observers.
Aims. We aim to explore the optical scattering-induced polarization that emerges from clumpy and warped dusty tori to check whether they can fit the unified model predictions.
Methods. We ran polarized radiative transfer simulations in a set of warped and non-warped clumpy tori to explore the differences induced by distorted dust distributions. We then included warped tori in a more complex model representative of an AGN to check, using polarimetry and imaging methods, whether warps can reproduce the expected polarization dichotomy between Seyfert-I and Seyfert-II AGN.
Results. The main results from our simulations highlight that isolated warped structures imprint the polarization degree and angle with distinctive signatures at Seyfert-I orientations. Included in an AGN model, the signatures of warps are easily (but not always) washed out by multiple scattering in a clumpy environment. Imaging polarimetry may help to detect warped tori, but we prove that warps can exist in AGN circumnuclear regions without contradicting observations.
Conclusions. Two warped tori with a non-significant difference in geometry in terms of photometry or spectroscopy can have entirely different signatures in polarimetry. Testing the geometry of any alternative model to the usual dusty torus using polarized radiative transfer is a necessary approach to verify or reject a hypothesis.

Key words. galaxies: active – galaxies: Seyfert – polarization – radiative transfer – scattering

1. Introduction

It is now commonly accepted that the innermost regions of active galactic nuclei (AGN) are surrounded by a parsec-scale optically thick equatorial distribution of dust. Antonucci & Miller (1985) found a Seyfert-I spectrum with broad emission lines, in the polarized optical light of the Seyfert-II galaxy NGC 1068, indicating that a Seyfert-I nucleus exists in all Seyfert-II AGN. The observational characteristics of Seyfert-IIs are in fact hidden from direct view by optically thick material. Radiation form the central engine is scattered onto the AGN polar outflows, resulting in the observed near-ultraviolet, optical and, near-infrared polarization properties. The idea of a common origin for emission lines for Seyfert-I and 2 galaxies, broad- and narrow-line radio galaxies, and quasars is supported by Shuder (1981). He found that Hα and other optical emission lines appear to correlate over a range of seven orders of magnitude with the continuum radiation. Subsequent recombinations that affect the emission lines might be uniform for almost all classes of AGN, but the presence of this hardly resolved dusty component is responsible for the observed orientation-dependent properties (Antonucci 1993; Urry & Padovani 1995).

Fortunately, the outskirts of the equatorial dusty medium of AGN start to be revealed thanks to the highest possible spatial resolution offered by interferometry. Recent Atacama Large Millimeter Array (ALMA) results showed that it is now possible to map the emission of the CO(6-5) molecular line and the 432 μm continuum emission from the nucleus of NGC 1068 (García-Burillo et al. 2016; Gallimore et al. 2016). In the mid-infrared, Jaffe et al. (2004) spatially resolved a parsec-sized torus-shaped distribution of dust grains in the same galaxy, where a small hot structure is embedded in a colder (320 K) dusty cocoon extending up to 3.4 pc in diameter. Further flux-limited interferometric studies of nearby quasars, using the MID-infrared Interferometric instrument (MIDI) at the Very Large Telescope Interferometer (VLTI; see, e.g., Tristram et al. 2007; Burtscher et al. 2009, 2013; Tristram et al. 2014) or the Keck interferometer (Swain et al. 2003; Kishimoto et al. 2009a), definitively confirmed the existence of the dusty torus, if with large differences within the sample.

The morphology of this region is a poorly constrained parameter of this multifaceted problem. The formation and hydrodynamic stability of a parsec-scale dust reservoir are not trivially explained by a homogeneous distribution of dust in a uniform toroidal arrangement. Detailed spatial studies revealed subtle problems with regard to smooth tori. Using *Spitzer* data, Sturm et al. (2006), Hao et al. (2007), Mason et al. (2009), and Nikutta et al. (2009) investigated the 10 μm silicate feature in a large sample of AGN. They found that the occasional detection of the feature in emission in Seyfert-II AGN, together with

the absence of any deeply absorbed features in Seyfert-Is, might rule out smooth density torus models. To suppress the emission feature, clumpiness is invoked (Nenkova et al. 2002, 2008a,b; Hönig et al. 2006; Schartmann et al. 2008; Stalevski et al. 2012). It is also a simple and elegant way to allow for the dust to survive the expected local temperatures. Krolik & Begelman (1988) postulated that the circumnuclear dusty material is likely clumpy, filled with a large number of individually optically thick clouds. Cloud merging and tidal shearing ensure a mixed environment that efficiently blocks radiation along the equatorial plane but allows a distant polar observer to see the central supermassive black hole (SMBH) through the dust-free funnel of the torus. Unfortunately, the exact geometry of the clumpy medium is beyond the resolution capabilities of current instruments. Infrared radiative transfer modeling has proven that multi-temperature multi-phase clumpy distributions can reproduce most of the observed characteristics of nearby AGN (Nenkova et al. 2008a,b; Stalevski et al. 2012). Similar results for the use of clumpy media instead of smooth density structures also emerged from polarized radiative transfer simulations (Stalevski et al. 2012). The near-infrared, optical, and ultraviolet polarization signatures of a complex AGN model including a clumpy dusty torus were found to be in agreement with the predictions from the unified model (Marin et al. 2015; Marin & Stalevski 2015).

If clumpiness is becoming more and more regarded as an important feature to add in (torus) simulations, there is another aspect of the unified model of Seyfert galaxies and quasars that is still barely investigated: the existence of warps. Using Very Long Baseline Array (VLBA) milliarcsecond-scale resolution observations of NGC 1068, Gallimore et al. (2004) revealed a slight misalignment between the line traced by the H_2O maser spots and the radio axis of the radio continuum source, believed to mark the location of the hidden nucleus. Very long baseline radio interferometry was also used to show that the accretion disk inside NGC 4258 may be a thin subparsec-scale differentially rotating warped disk (Herrnstein et al. 1999).

Misaligned or warped structures have been detected in a variety of sources and can be imaged with great precision for disks around nearby stars, such as in the case of HD 142527. Marino et al. (2015) used polarized differential imaging to detect a warp in the outer disk of the HD 142527 system, thanks to the shadows cast by the inner disk. Secular perturbations of a planet can also affect the inclinations (i.e., orbital plane) of nearby planetesimals. Introducing a planet into the disk on an orbit inclined to the disk midplane causes a warp to propagate away from the planet (Augereau et al. 2001). In the case of galaxies, Caproni et al. (2004) and Caproni & Abraham (2004) reported observational evidence of spin-induced disk/jet precession. This precession may lead to a warp of the innermost part of the AGN accretion disk with respect to the outer parts due to the Bardeen-Petterson effect (Bardeen & Petterson 1975). Warps can also be created at larger distances from the potential well by nonaxisymmetric magnetorotational instability (Menou & Quataert 2001) as well as the Kelvin-Helmholtz instability (Gunn 1979). The presence of shear motion inside the torus works as an agent to drive Kelvin-Helmholtz instabilities, resulting in the generation of a strong wind and potential warps (Gunn 1979; Kiuchi et al. 2015). Such warps would be difficult to detect in photometry, spectroscopy, or imaging in galaxies that are not nearly edge-on (Meyer 1989), but polarimetry could be the answer.

The discovery of a polarimetric dichotomy between Seyfert-I and Seyfert-II was the most important proof for the establishment of the unified scheme (Antonucci 1993). Optical polarization from Seyfert-Is is mostly <1% and parallel to the projected radio axis of the system (its polarization position angle PPA is thus equal to 90°), while Seyfert-IIs are always showing a polarization degree >10% with polarization angle = 0° (perpendicular polarization). This dichotomy is due to the presence of the circumnuclear dust material that prevents direct radiation from escaping from the equatorial plane in edge-on systems. Scattering inside the polar outflows results in higher polarization degrees P and a perpendicular polarization, driven by the angle-dependence of Thomson scattering. This observational (Antonucci 1984) and theoretical (Wolf & Henning 1999; Young 2000) model works very well for smooth density and clumpy tori (Marin et al. 2012, 2015) but would warped dusty tori fit in this picture? Could they account for the high perpendicular polarization found in Seyfert-IIs? And would they reproduce the observed polarization dichotomy? The latest papers on warped structures around the innermost regions of AGN do not answer these questions, and they are the goal of our present work.

Accounting for both non-smooth density distributions and warps, we aim to test whether warped media can affect the optical continuum polarization of a complex AGN model. We wish to determine whether warps and misaligned structures at the torus distances can fit the unified model, such as postulated by Lawrence & Elvis (2010), or if caution must be taken when dealing with deformed tori. To do so, we construct a simple toy model for warped tori in Sect. 2, where we present the formalism and the Monte Carlo radiative transfer code used in our simulations. It is not our ambition to provide an accurate physical model for warped structures; this should be done together with hydrodynamical simulations (e. g., Wada et al. 2016). In Sect. 3 we test our clumpy and warped torus and compare the results to non-warped structures. We explore the space of parameters used to create the warp and show that warps have a profound impact on isolated tori. We include the warped structures in more complex AGN models in Sect. 4, taking into account polar outflows and equatorial inflows. We create imaging polarimetry maps of an AGN with a warped torus before exploring another model for a warped uniform dusty torus in Sect. 5. We discuss our results and further progress to be made in Sect. 6 before concluding in Sect. 7.

2. Modeling warped and clumpy dusty tori

One of the most common geometries used to represent the circumnuclear dusty material in AGN is a torus (see the earliest representations in Antonucci 1984, where the outer boundary of the equatorial region was not drawn due to the lack of information on that point). Other morphologies, such as flared dusty disks, representative of outflowing material, are sometimes used in infrared studies (e.g., Manske et al. 1998; Stalevski et al. 2012), but give similar spectroscopic results to dusty tori. For a polarimetric investigation of the differences between a clumpy flared disk and a clumpy torus, see Marin & Stalevski (2015). In this paper, we focus on a toroidal structure that is warped at a given distance from the center of the model (where the SMBH lies).

2.1. The clump distribution

We first consider a regular torus with an elliptical cross-section, ranging from an inner radius $R_{\rm in}$ = 0.1 pc to an outer radius $R_{\rm out}$ = 5 pc. The inner radius was fixed according to the dust sublimation radius for a $\sim 10^7$ $M_\odot$ SMBH with sub-Eddington accretion rate. $R_{\rm sub}$ is correlated to the UV/optical continuum emission ($L_{\rm bol}/L_{\rm Edd}$ = 0.45, see Kollmeier et al.

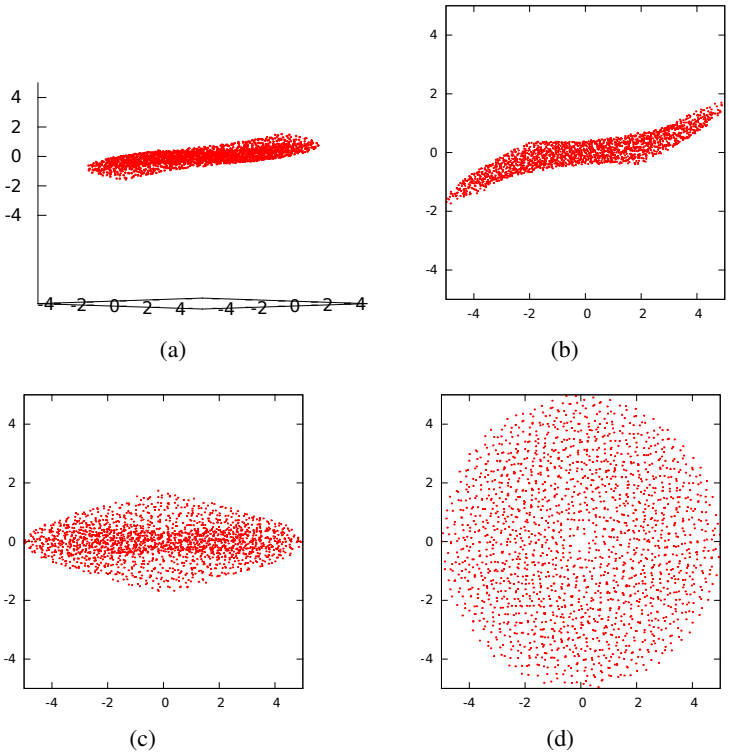

Fig. 1. Representations of a clumpy warped dusty torus with $R_{\rm warp}$ = 2 pc and $\theta_{\rm warp}$ = 30°. Axes are in parsecs. The *top left panel* is a three-dimensional view of the model; *top right*: projection onto the *xz*-plane (Seyfert-II view, azimuthal angle = –90°); *bottom left*: projection onto the *yz*-plane (Seyfert-II view, azimuthal angle = 0°); and *bottom right*: projection onto the *xy*-plane (Seyfert-I view).

2006) and to the sublimation temperature $T_{\rm sub}$. The latter was fixed to 1500 K, a value that accounts for the temperature range of ambient gas pressures for both graphite and silicate grains (Kishimoto et al. 2007). The outer torus radius corresponds to the typical extent of compact and optically thick tori in nearby AGN, ranging from 1 to 10 pc according to simulations (Pier & Krolik 1992; Siebenmorgen et al. 2015) and observations (Tristram et al. 2007; Kishimoto et al. 2009b). The torus half-opening angle was fixed to 30° from the equatorial plane, a value chosen to agree with observed half-opening angles of the equatorial AGN region recently estimated by Sazonov et al. (2015) and Marin & Antonucci (2016). The toroidal structure was then filled with constant-density spheres with radius 0.11 pc (Stalevski et al. 2012). Each clump had an optical depth of 50 in the *V* band, so a single cloud can efficiently obscure the central AGN engine in the optical band (Siebenmorgen et al. 2015). The dust mixture had a composition similar to the Milky Way dust (Mathis et al. 1977). We note that the choice of a Milky Way dust mixture instead of a Small Magellanic Cloud-like dust composition, for instance, where the dust is smaller than that in the Galactic diffuse interstellar medium, ISM (Prevot et al. 1984), does not change the outcomes of the simulations in the optical band as scattering in opaque dust clouds produces relatively gray scattering (Kishimoto et al. 2001). We fixed the number of clouds to 2000 in order to have a volume-filling factor of 22−23% (the spherical clouds do not overlap, see also Stalevski et al. 2012). This model is the basis of all models we explore in the forthcoming sections, and we study it Sect. 2.3 as a test case.

To create warps in this structure, we defined a radius $R_{\rm warp}$ at which the clumps depart from the torus structure. When a clump is generated at a distance larger than $R_{\rm warp}$, its *z*-coordinate is shifted upward or downward according to its position on the *xy*-plane:

$$z = \pm\left[z + \left(\sqrt{x^2+y^2} - R_{\rm warp}\right)\tan(\theta)\right], \quad (1)$$

with

$$\theta = \frac{2\times\theta_{\rm warp}\left(\frac{\pi}{2} - \arctan\left(\frac{|y|}{|x|}\right)\right)}{\pi}. \quad (2)$$

$\theta_{\rm warp}$ is the maximum warping angle, that is, the angle between the equatorial plane and the warped torus in the *xz*-plane. A torus warped through angle $\theta_{\rm warp}$ will intercept and reradiate a fraction close to $\theta_{\rm warp}/3$ of the luminosity of the central source (Phinney 1989). A visual representation of a warped torus with $R_{\rm warp}$ = 2 pc and $\theta_{\rm warp}$ = 30° is shown in Fig. 1. The top left panel is a three-dimensional view of the model with 2000 clumps (clump sizes not to scale). The other three panels show the projection of the warped torus structure onto the *xz*, *yz*, and *xy*-planes. The distance at which the warping effect starts is shown in Fig. 1b, together with the warping angle $\theta_{\rm warp}$. In Fig. 1c, we show a denser region close to the equator, which is the inner part of the torus that is unaffected by the warping effect. Finally, panel (d) is a view from the top, and it is impossible to detect the warp.

This simple warping method has several advantages: the outer radius of the dusty torus is the same regardless of the azimuthal angle of the observer, so Seyfert-Is with low inclinations (<10°) should not lead to excessively elongated dust lanes along any directions. Only the height of the structure is affected, resulting in possible polar dust signatures for intermediate and Seyfert-IIs, far beyond the torus height defined by its half-opening angle (Bock et al. 2000; Burtscher et al. 2013). Polar mid-infrared emission from this type of warped dust distribution

could contribute to the important polar infrared flux discovered by interferometry studies of Seyfert-IIs with high position angle and baseline coverage (Tristram et al. 2014; Asmus et al. 2016; López-Gonzaga et al. 2016). The antisymmetry between the upper and lower parts of the warped structure naturally arises even under these simple conditions. This could be due to a strong radiation field or an outflow dense enough to wipe the external surface of the circumnuclear dust, but they must sustain a small deflection with respect to the torus axis. This is the basic idea developed in Pringle (1996), Nayakshin (2005), and Lawrence & Elvis (2010); see Figs. 5 and 6 in Lawrence & Elvis (2010) for illustrations.

There are other methods to warp tori. Recently, Jud et al. (2017) investigated uniform, geometrically thin, warped dusty disks in the infrared band using a disk modified to have a concave shape at small radii that turns over at large radii. Their final structure is similar to what is being investigated here, with differences in the temperature profile and bulk shape of the disk at $R > R_{\rm warp}$. Since we explore the optical scattering-induced linear polarization of warped tori in this paper, the temperature profile has very little influence onto the scattered radiation. An important difference is that our modeling includes clumpiness, a critical aspect that would change the shape of the silicate feature and the spectral energy distribution in the infrared band (Jud et al. 2017, and references therein). However, we note that our model was not checked for consistency with the infrared emission expected from Seyferts, for example, the silicate feature strengths or interferometry results. Our goal is not to present a new warping method, but to check whether warped tori can exist within the unified AGN picture, based on polarimetric observations.

2.2. Radiative transfer with STOKES

Radiative transfer was achieved using the Monte Carlo code STOKES, a simulation tool that was written to investigate the polarization signature of AGN in the optical and ultraviolet bands (Goosmann & Gaskell 2007). The code was later improved to provide imaging analysis (Marin et al. 2012) and clumpy reprocessing regions (Marin et al. 2015). A summary of the code performances can be found in Marin & Goosmann (2014). The three-dimensional capabilities of the code allow exploring an AGN model without any symmetries by virtually revolving around. For the remainder of this paper, we investigate three different inclinations: 18° (Seyfert-I view), 50° (intermediate inclination), and 87° (Seyfert-II view).

The photon source used in the simulation is a point-like source of isotropic emission. The initial radiation is unpolarized and fixed at a monochromatic wavelength of 5000 Å (B/V-band). Around the central source are the reprocessing regions that can scatter, absorb, or re-emit radiation. Mie and Thomson scattering are accounted for but the code does not handle temperature variation due to dust being heated or grain cooling by emission at infrared wavelengths. Re-emission from dust is thus not treated in theses simulations, which is a non-vital simplification as dust re-emits at much longer wavelengths than in the blue and visual bands. The four Stokes parameters of light (Stokes 1851) are recorded, but we focus on linear polarization, since optical circular polarization from AGN was much less frequently investigated by observers. As the Monte Carlo method employs a stochastic approach, the results obey Poisson statistics. We set the number of photons to be simulated in order to have small (<1%) statistical fluctuations per direction bin. Hence, each simulation sampled $\sim 10^9$ photons for a computational time of 96 h per model[1].

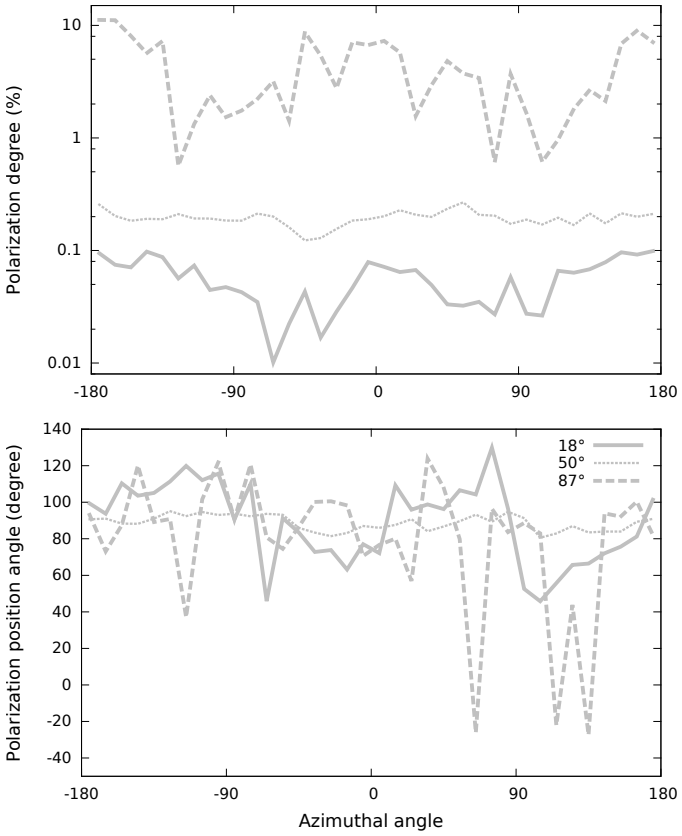

Fig. 2. Optical polarization (5000 Å) from a clumpy dusty torus without warping effects. The *top panel* shows the polarization degree P and the *bottom panel* the polarization position angle PPA. The lines refer to the inclination of the model: the solid line indicates a viewing angle of 18° (Seyfert-I view), the dotted line an intermediate inclination of 50°, and the long dashed line a viewing angle of 87° (Seyfert-II view).

2.3. Test case: a clumpy dusty torus without warps

Before exploring the optical scattering-induced linear polarization from warped and clumpy dusty tori, the test model presented in Sect. 2.1 was investigated. This test case is a clumpy torus model without warp and is similar to what has been studied in Marin et al. (2015). The effects of the clumpiness of the torus in a direct comparison with a continuous torus have been already presented in Marin et al. (2015) and Marin & Stalevski (2015). The results are shown in Fig. 2: the top graph presents the polarization degree P as a function of the azimuthal angle for three different inclinations i. The chaotic variations in P are not due to insufficient Monte Carlo statistics. They are due to the clumpiness of the circumnuclear region: as the circumnuclear torus was randomly filled with clumps, each azimuthal angle sees the central source with a different covering factor. The photon trajectories and the absorption probabilities vary from two consecutive bins separated by an angle of 1 degree, resulting in the observed variations in P. The linear polarization is also

[1] Radiative transfer simulations are time-consuming, especially when clumpy media are involved. After emission or a scattering event, STOKES checks if a clump lies along its direction. As there are thousands of clumps in the model, the checking procedures drastically increases the duration of the simulations.

inclination dependent, with $P < 1\%$ for Seyfert-I inclinations and $P < 10\%$ at Seyfert-II inclinations. Compared to the pole-on and edge-on views, the intermediate inclination polarization curve appears smoother in azimuth dependence; this effect is due to a lesser influence of clumpiness onto the $i = 50°$ case. At the transition angle between Seyfert-Is and Seyfert-IIs, back scattering onto the torus funnel is contributing the most to the polarization signal: in this case, the photon only "sees" a convex wall of dust and, if not absorbed, backscatters toward the observers, regardless of the existence of clumps behind the first cloud. An azimuthal-integration of P gives the following average values: 0.04% at $i = 18°$, 0.19% at $i = 50°$, and 2.61% at $i = 87°$. Since the variations of the non-warped model are caused by the random clump distributions, we used these integrated values for comparison purposes with our following models (see next section).

Similar conclusions can be drawn from the polarization position angle (PPA, bottom panel), which is mainly parallel to the symmetry axis of the model (hence yielding a value close to 90° when azimuthally integrated). This is the averaged polarization angle that has been found in previous modeling with geometrically flat clumpy tori, see Marin & Stalevski (2015) and Fig. 5 in Marin et al. (2015). What is shown here and not in the previous publications is that the PPA can rotate by 90° when the covering fraction of the source is insufficient at Seyfert-II inclinations. This effect is strengthened by the fact that there is no diffuse inter-clump medium that would prevent or attenuate the propagation of photons in edge-on orientations. A second feature of interest for the remainder of the paper is that the PPA can be offsetted by 0 to 30° from parallel polarization at a given phase, simply because of the random clump distribution.

The results from the test case seem to contradict the observations, where Seyfert-IIs should have $P > 10\%$ and PPA $\sim 0°$, but we recall that it is only because the torus is isolated from the rest of the usual AGN components. We show in the following sections that including polar winds drastically changes the picture.

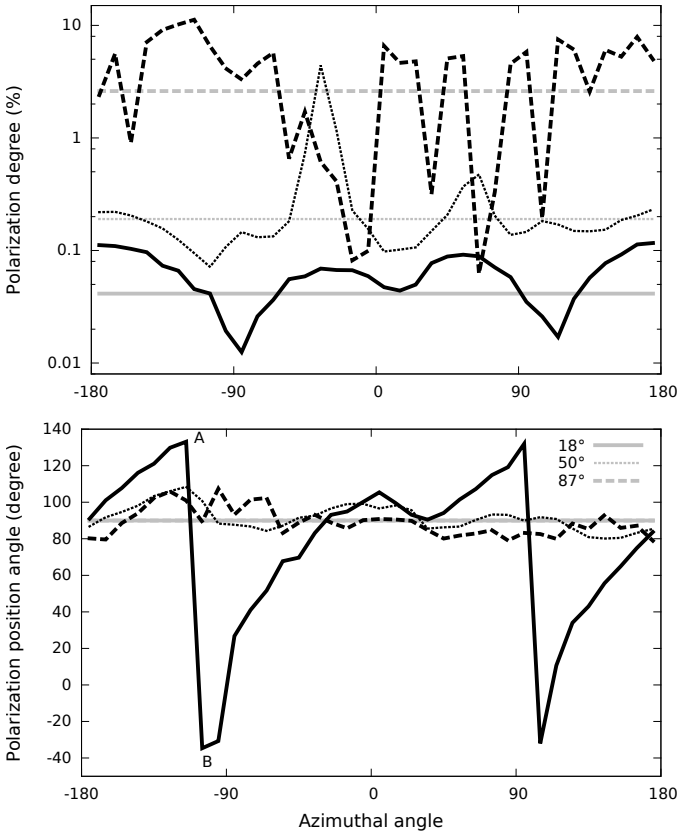

Fig. 3. Optical polarization (5000 Å) from a warped and clumpy dusty torus (in black) with $R_{\rm warp} = 2$ pc and $\theta_{\rm warp} = 30°$, overplotted onto the azimuthally integrated polarization from the test model (in gray). The *top panel* shows the polarization degree P and the *bottom panel* the polarization position angle PPA. Points A and B mark the azimuthal bins before and after the large amplitude variation in PPA discussed in the text and developed in Fig. 4. The legend is the same as in Fig. 2.

3. Optical polarization from clumpy and warped tori

3.1. Results for a specific parametrization

In the previous section, we obtained the optical scattering-induced polarimetric signature of a clumpy toroidal structure and saw that chaotic variations in P and PPA naturally arise from the random distribution of dust clumps that only fill 22−23% of the total volume. We now add a warp that starts at a distance of 2 pc from the center of the model. The warp has an angle of 30° with respect to the equatorial plane, thus reaches a maximum height of 1.73 pc above the midplane (see Fig. 1b).

Compared to the test case, a warped clumpy torus (Fig. 3) shows remarkable signatures in both P and PPA at a Seyfert-I inclination. The PPA presents sawtooth oscillations with sharp inversions around azimuthal angles −90° and +90°, associated with local minima in P. The polarization angle modulation can be as high as 180° due to the maximum asymmetry seen by a distant observer[2]. The bottom part of the warp being hidden by the equatorial dust content at $i = 18°$, only the side of the warp that faces the observer contributes to the net polarization, resulting in azimuthal-dependent PPA. This effect is much less pronounced at intermediate and equatorial inclinations: the inner parts of the clumpy structure efficiently block radiation, and the specific sawtooth oscillations are smoothed out. Compared to the test model, the scatter in PPA for the warped torus appears smaller at equatorial inclinations. Polarization mainly arises from backscattering from the torus funnel and the contribution of the warped and distant surfaces is negligible (as is confirmed by imaging polarimetry results, see Sect. 4.2). At these inclinations, the averaged P for a warped dusty torus is marginally higher than what has been found for a non-warped model. Even when P shows more scatter around the mean for the warped model, we may estimate its averaged values: 0.06% at $i = 18°$, 0.34% at $i = 50°$, and 4.23% at $i = 87°$.

We further investigated the sharp variation in PPA by examining the model from a wider range of inclinations. In Fig. 4 the rotation of the polarization angle close to the minimum of the sawtooth (~90° phase, between points A and B in Fig. 3) is shown in black. The code has difficulties to sample inclinations lower than 8°, but it is clear that the largest PPA variations occur at polar inclinations. The increasing importance of backscattering from the torus funnel at inclinations $i \geq 25°$ stabilizes the polarization angle at low polarization modulations; the PPA values are consistent with clump-induced effects, as discussed in the last point in Sect. 2.3. The inclination at which the PPA flattens is consistent with $\theta_{\rm warp} = 30°$, accounting for the effects of clumping. At $i = 60°$, torus obscuration starts, but the gap between the clouds allows radiation to escape easily. At $i \geq 65°$, the

[2] The polarization position angle is periodic. Any polarization ellipse is indistinguishable from one rotated by 180°, which is one of the fundamental advantages of radio antenna polarimetry. The sawtooth pattern is caused by this periodicity; an observer is expected to see a continuous increase of the PPA with a polarization modulation.

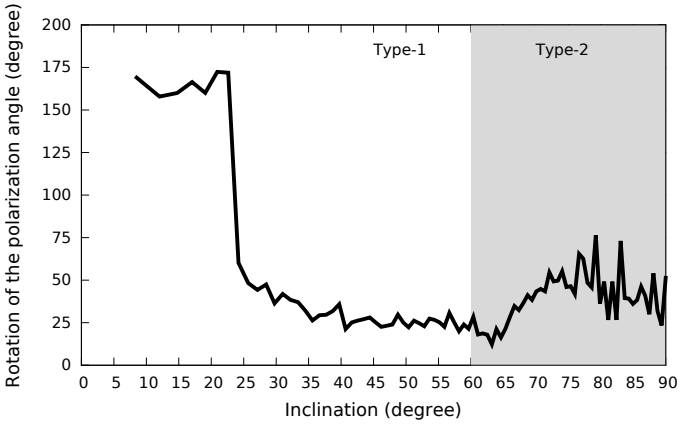

Fig. 4. Rotation of the PPA between points A and B (see Fig. 3), corresponding to the difference between maximum and minimum values of the PPA at azimuthal angles close to −90°. The polarization angle modulation is shown for every inclination of the observer. The shaded gray area represents the line of sight obscured by the clumpy equatorial dust distribution, setting the boundary between Seyfert-Is and Seyfert-IIs (the later type being in the gray area).

PPA again starts to oscillate because of the growing influence of equatorial obscuration. Only the fraction of the torus funnel that is opposite to the observer and the far end of the warped structure are scattering photons, but the resulting polarization angle is still dominated by multiple scattering effects. Thus, clumpiness has a much more important impact than warps on polarization at intermediate and edge-on orientations.

3.2. Exploring the parameter space

Two important parameters drive the warp structure: the distance at which the warping effect starts ($R_{\rm warp}$), and the maximum angle between the equatorial plane and the warped structure ($\theta_{\rm warp}$). Both can be used as tracers of the initial non-axisymmetric phenomenon that leads to torus warping, but the question is whether they can be estimated from polarimetric measurements. In this subsection, we run a grid of warped tori varying $R_{\rm warp}$ and $\theta_{\rm warp}$, and we examine the resulting polarization as a function of azimuthal angle. The results are summarized in Figs. 5 and 6 for the polarization degree and the polarization angle, respectively.

The first and probably most important observation is that a warped dusty torus always drives 180° rotations of the polarization angle at Seyfert-I orientations when revolving around the structure. The sawtooth polarization modulations in PPA are associated with local minima in P, such as seen in Fig. 3, that can decrease P by one order of magnitude in the most extreme case. The azimuthal angle at which the polarization modulation occurs does not change gradually as a function of both $R_{\rm warp}$ and $\theta_{\rm warp}$; it cannot be easily predicted. The random sampling of the density distribution/clumpiness creates higher- and lower-density subregions, resulting in enhanced asymmetry, and partly offset from 90° in azimuthal angle the minima in P and PPA. Regardless of the configuration of the warp, the sawtooth rotations of the PPA are a clear and distinct signature of isolated warped tori. The averaged polarization degree for warped tori at Seyfert-I inclinations ranges from 0.04% to 0.12%. These values are slightly higher than what was found for non-warped non-clumpy torus models (Goosmann & Gaskell 2007), as asymmetry is enhanced here. At other inclinations, PPA flattens around 90° as a result of the randomization of the clump positions and multiple scattering that tend to hide potential $P(R_{\rm warp}, \theta_{\rm warp})$ or PPA$(R_{\rm warp}, \theta_{\rm warp})$ correlations. Variations in the covering fraction of the source at different azimuthal angles have a much deeper effect onto the continuum polarization than warps. The averaged polarization degree for warped tori at intermediate inclinations ranges from 0.13% to 0.62%; for edge-on systems, P ranges from 3.41% to 5.61%, which is in agreement with past polarimetric modeling (Marin et al. 2015).

4. Impact of warped dusty tori in a global AGN model

We can summarize our current results by stating that warps do not strongly affect the polarimetric signatures of clumpy dusty tori at intermediate and edge-on inclinations. The signatures of warps in the dust structure are washed out by the polarization emerging from reprocessing on the equatorial distribution of clumps. However, at Seyfert-I inclinations, there is a tremendous impact of warps onto the polarization position angle. This 180° polarization modulation occurs in the case of isolated warped structures, but does this feature also impact a complex AGN model where inflowing material from the torus connects to the broad line region (BLR), where ionized polar outflows extend up to tens of parsecs? Moreover, can warped and clumpy dusty tori account for the high perpendicular polarization found in Seyfert-IIs? It is the aim of the next section to answer these fundamental questions.

4.1. Polarization from an AGN with a warped equatorial obscurer

To investigate a complex AGN model, we added two components to the previous warped and clumpy dusty tori: an equatorial electron-dominated inflow, and a polar biconical structure representative of the ionized winds. The former region represents the accretion flow between the torus and the BLR, a necessary structure used to reproduce the observed polarization dichotomy in AGN (Young 2000; Goosmann & Gaskell 2007). The equatorial region is a flared disk with half-opening angle 20° from the equatorial plane and models a radiation-supported disk structure. It spans from 0.03 to 0.05 pc and is filled with electrons, such that the V-band optical depth along the equator is 1 (Marin et al. 2012). This equatorial inflow should not be confused with the BLR, where most of the material is neutral (as evidenced by fast variations in the neutral absorbing column seen in X-ray observations, e.g., Maiolino et al. (2010) or Netzer (2013) for models). The second structure is an electron-filled hourglass-shaped wind that is outflowing from 0.1 to 30 pc from the center of the model. The optical depth of the wind is fixed to 0.05, a representative value of the optically thin polar regions observed in nearby Seyferts (Miller et al. 1991). Increasing the optical depth contributed by the narrow-line region to values higher than 0.05 (such as presented in Fig. 3 in Schnorr-Müller et al. 2016, where a typical A_V of 1–2 mag is found) will not change the outcome of the simulation as long as the optical depth remains lower than unity. Otherwise, multiple scattering in a Thomson-thick electron medium will increase the number of scatterings needed by radiation to escape the model along Seyfert-I viewing angles, rotating the final polarization position angle by 90° (see Marin et al. (2012) for a grid of AGN polarized simulations with the polar winds V-band optical depth ranging from 0.01 to 3).

Our grid of results is presented in Figs. 7 and 8 for the polarization degree and the polarization position angle, respectively.

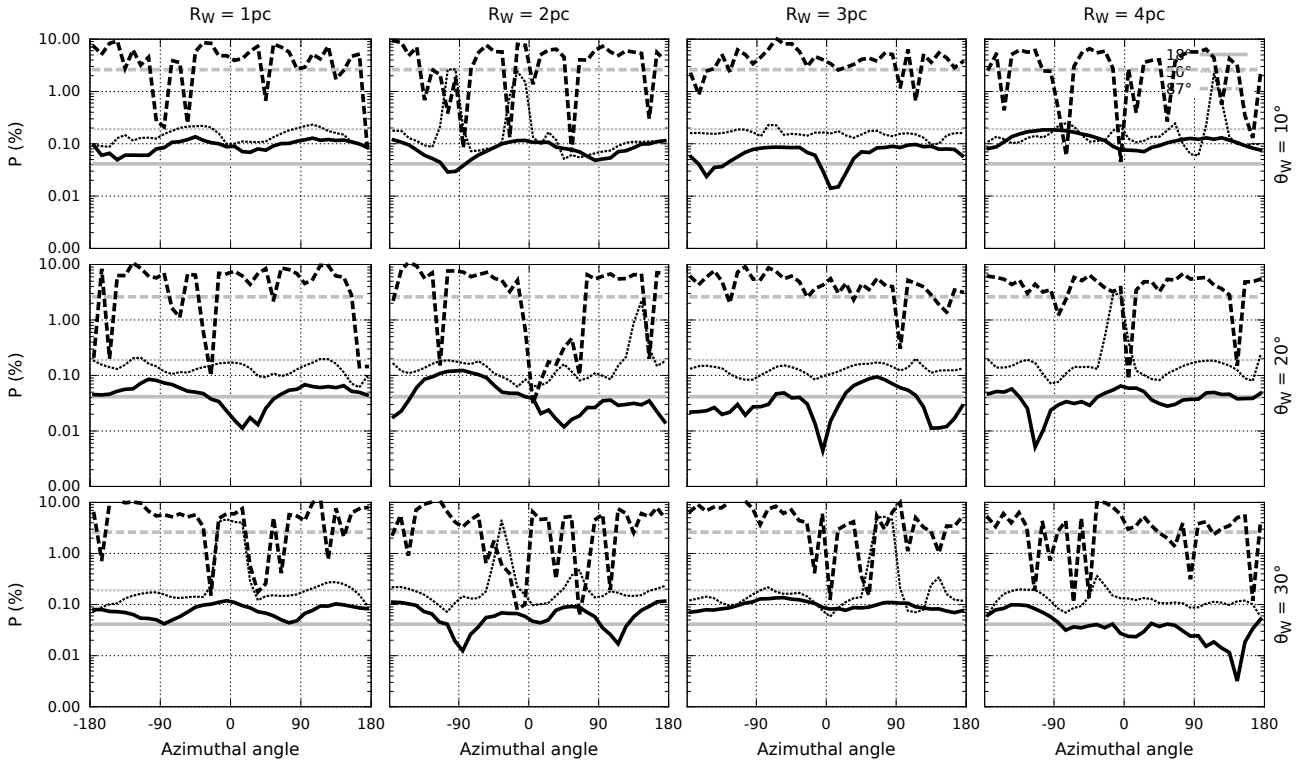

Fig. 5. Resulting percentage of polarization P as a function of viewing angle (solid line: 18°, dotted line: 50°, and long dashed line: 87°) and azimuthal angle for a set of warped and clumpy dusty tori. The legend is the same as in Fig. 2.

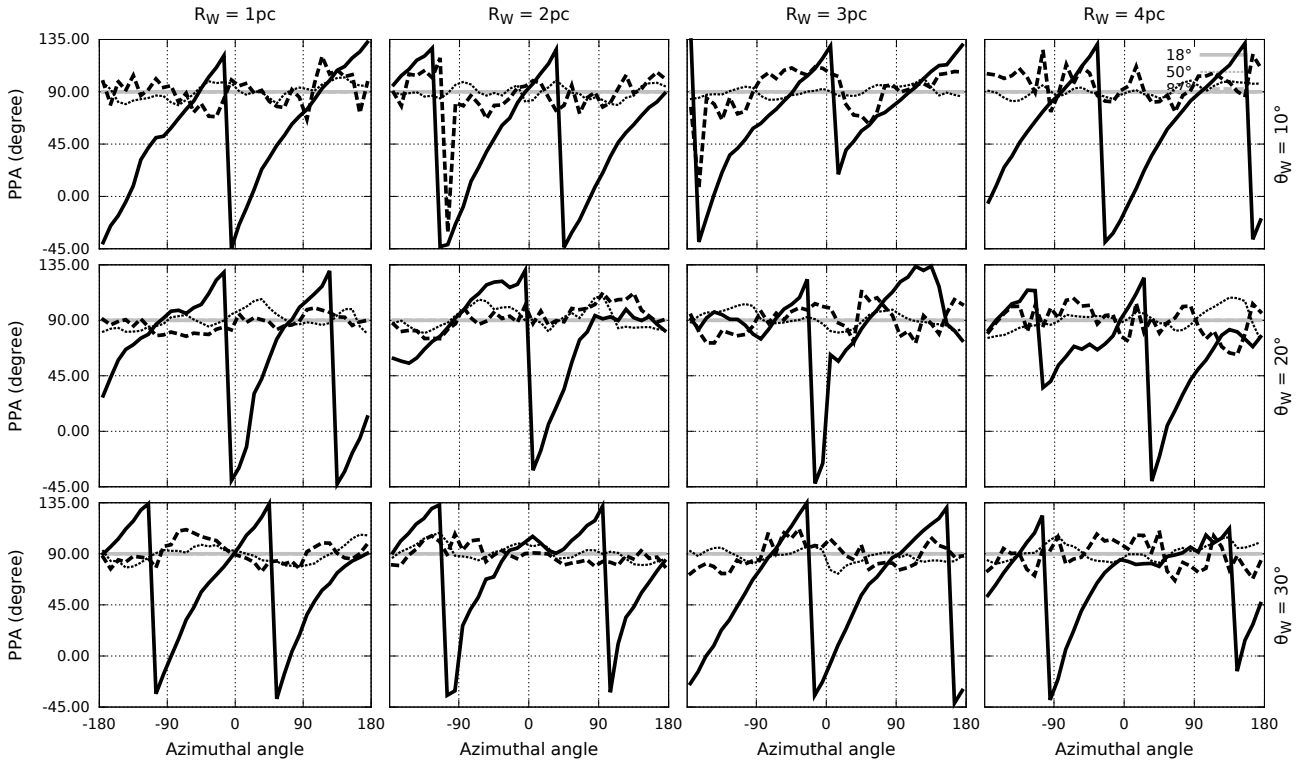

Fig. 6. Same as Fig. 5, except that the polarization position angle PPA is shown here.

Focusing on Seyfert-I inclinations, we see that both P and the PPA are azimuthally independent. The polarization degree resulting from scattering in a complex AGN model with a warped torus is on the order of 0.4%. Scattering off the radiation-supported inner disk provides most of the polarized information and the amount of secondary or tertiary reprocessing onto the dusty equatorial structure is not sufficient to impact the net P, nor the PPA, which is fixed to 90° (parallel polarization). Electrons in the polar winds do not contribute to P as the medium is optically thin, and forward-scattering leads to small degrees of

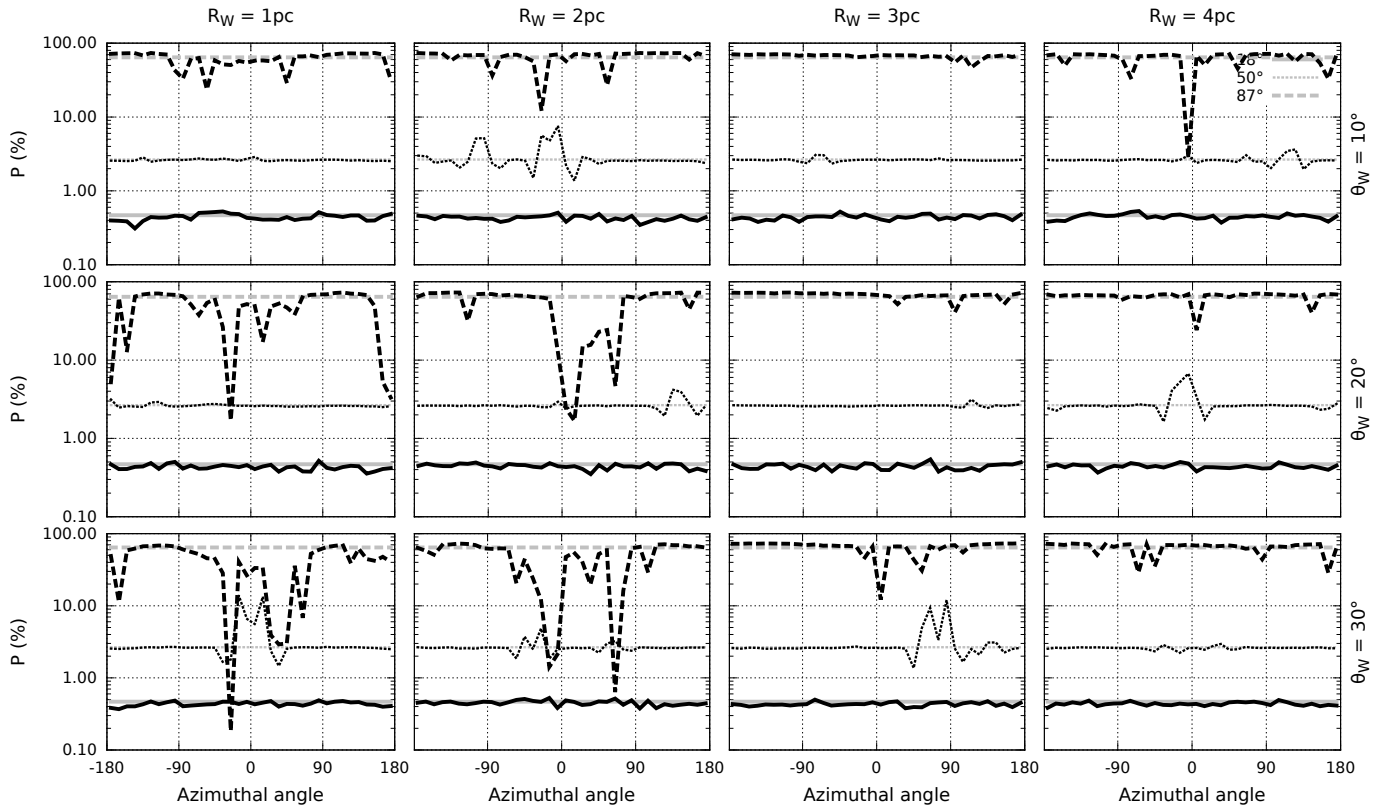

Fig. 7. Resulting percentage of polarization P as a function of viewing angle (solid line: 18°, dotted line: 50° and long dashed line: 87°) and azimuthal angle for a set of complex AGN models (see text) using the same warped and clumpy dusty tori as in Fig. 5. Tthe black and gray lines both describe the complex AGN model, but the gray line is the result of an azimuthal integration (fine details are thus washed out). The rest of the legend is the same as in Fig. 2.

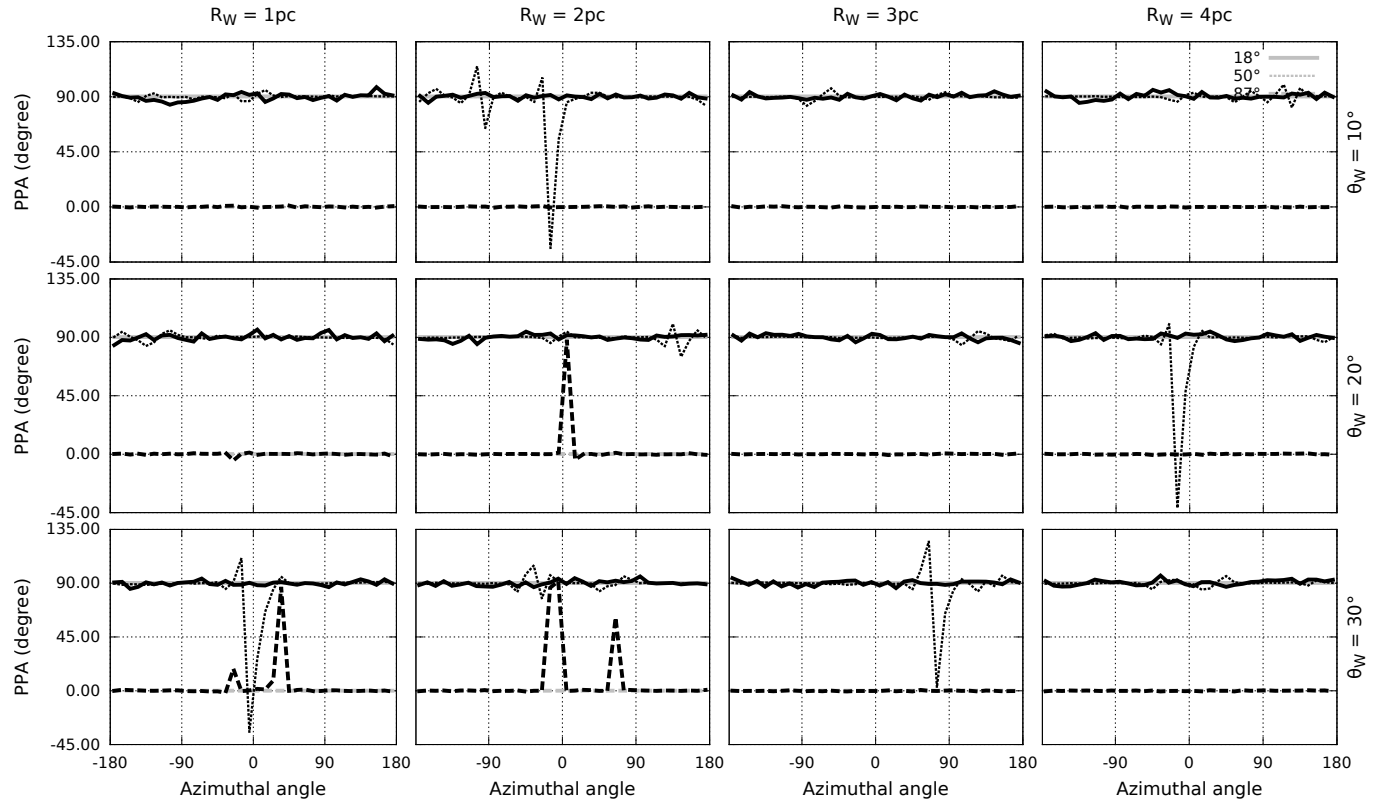

Fig. 8. Same as Fig. 7, except that the polarization position angle PPA is shown here.

polarization. This type of signature is the same that was found by previous authors when modeling smooth-density or clumpy distributions of matter in complex AGN models (Kartje 1995; Marin et al. 2012, 2015). This is also the typical amount of polarization found in nearby Seyferts that are dominated by equatorial-scattering (Smith et al. 2002).

The case of an intermediate inclination is similar: the polarization position angle is almost always parallel to the symmetry axis of the model, with polarization degrees of between 2 and 3%. However, in rare cases, the polarization angle rotates by ~90°, driving oscillations in the polarization degree (see, e.g., the case $R_{\rm warp} = 3$ pc and $\theta_{\rm warp} = 30°$ in Figs. 7 and 8). This phenomenon is due to the occultation of the central region by a single or a group of dusty clouds. Scattered radiation from the wind will then prevail and rotate the PPA, impacting P. The polarization degree first decreases when the PPA rotation occurs, then reaches a maximum (<10%), then decreases again when the PPA stabilizes again. Most of these PPA variations occur at an azimuthal angle close to 0°, when the upper part of the warp (with positive z coordinates) can intercept the observer's viewing angle.

The case seems more complex for Seyfert-II inclinations. If the polarization degree is indeed high due to Thomson scattering in the polar winds, leading to PPA = 0° such as expected from Seyfert-IIs (Antonucci 1993), it may also show orthogonal rotations when the clump distribution is not dense enough to entirely cover the central region. Scattered radiation from the equatorial plane will dominate and rotate the polarization angle, decreasing the net polarization degree (the inverse phenomenon described for intermediate inclinations). However, variations in P are not always related to PPA oscillations: the warped structure, extending higher from the equatorial plane than a regular torus, may contribute to the global polarization by scattering photons that emerge from the dust funnel or from the radiation-supported disk. The mainly parallel polarization angle of these photons will mix with the perpendicular signature of photons scattered in the polar region and thus cancel P. The contribution of the radiation with parallel PPA is weaker, thus P does not completely cancel out, but it might be significant enough to bring the polarization degree to several percent. Coupled to the clumpiness effect and the partial covering of the nucleus, P can be as low as 0.2%. This case is statistically very unlikely, otherwise AGN with optical Seyfert-II classifications but Seyfert-I polarization degree and angle would have been observed yet (Antonucci 1993).

4.2. Imaging polarimetry

Revealing the polarization pattern around the hidden nuclei of Seyfert-IIs was a major success when the polarimeter on board the *Hubble* Space Telescope was available and helped the community to better understand the morphology and composition of the resolvable structures surrounding the obscured SMBH. In particular, imaging polarimetry helped to localize the position of the hidden source of UV continuum, highlighted the shape of the ionized polar winds, detected dichroic signatures in linear polarization, estimated the amount of foreground extinction, examined the composition of the NLR led to refined AGN models by better constraining the distribution of the scattering medium (see Capetti et al. 1995, 1996, and more recently Gratadour et al. 2015, with the Spectro-Polarimetric High-contrast Exoplanet REsearch instrument (SPHERE) on the Very Large Telescope, VLT). Polarization induced by dust scattering onto the circumnuclear region has been undetectable so far and will remain impossible to resolve for many years because of the small amount of flux that is reprocessed by this region and because of the technical limitations of current facilities. As an example, under decent atmospheric conditions, a maximum of 60 milliarcsec (~4 pc) resolution for imaging polarimetry is achievable on NGC 1068 ($d = 14.4$ Mpc) in the H and K bands using adaptive optics (Gratadour et al. 2015). On the other hand, General Relativity Analysis via VLT InTerferometrY (GRAVITY) at the VLTI (in the K band) has an imaging resolution of about 2 mas and may be able to measure polarization in a few bright AGN thanks to its Wollaston prism (Gillessen et al. 2006). Yet, observations will be limited to very few sources and the polarized signal from the torus might be diluted by the emission from the cones. However, if the torus is warped and extended along the polar regions, it might be possible to detect some effects on the AGN polarization maps.

To investigate the impact of warped tori, we ran the AGN model presented in Sect. 4.1 using the following warp parametrization: $R_{\rm warp} = 2$ pc and $\theta_{\rm warp} = 30°$. We created the polarization maps of the AGN at the same three viewing angles as shown in all the figures of this paper (18°, 50° and 87°), together with three azimuthal angles (0°, 45°, and 90°). The polarized flux maps are presented in Fig. 9, the polarization fraction maps in Fig. 10, and the polarization position angle maps in Fig. 11. The spatial resolution of the images is 200×200 pixels, which, for an NGC 1068-like AGN distance would give a pixel size of 0.11×0.11 pc (0.1 arcsec $\approx 11\ h_{50}^{-1}$ pc, see Capetti et al. 1995). The (0,0) coordinates give the position of the central SMBH.

As the imaging polarimetry (Figs. 9–11) shows, most of the polarized flux emerges from the circumnuclear dust funnel and propagates through the wind. Forward-scattering inside the wind occurs too rarely to impact the larger amount of flux that has scattered inside the inner dust radius or propagated into the torus and then escaped along the polar direction. Equatorial scattering thus imposes its PPA, as Fig. 11 shows. The net polarization degree is diluted by unpolarized radiation from the source, resulting in low values (Fig. 10). The elongated shape of the spot of maximum flux is due to the inclination of the system in addition to backward-scattering of photons from the torus to the observer. Thanks to the gaps between the clouds, photons can journey farther into the dust medium than in the case of a smooth-density distribution, but their polarization signature has no global impact (Marin et al. 2015). The warps are not easily detected from imaging polarimetry of Seyfert-Is. For intermediate inclinations, the line of sight of the observer is not obscured by the equatorial dust. The inner region shines and its polarization dominates over the polarization resulting from wind interactions. This is a visual confirmation of the results presented in Figs. 7 and 8. The warp can be distinguished in the maps (middle-right images) as an extension toward the left of the image. This extension is particularly visible in the polarization degree and polarization angle maps, while as a result of the small amount of scattered radiation, it can be missed in the polarized flux maps. Without prior information, it is impossible to determine whether this material is an isolated dust lane or part of the dusty structure. The warp that is situated beneath the equatorial plane is invisible. At Seyfert-II inclinations, the warp has a direct impact onto the polarization maps. At an azimuthal angle of 0°, when the warp maximum polar elongation faces the observer, an important fraction of the wind base is obscured, and there is an asymmetry in the polarized flux detected from the northern AGN part with respect to the southern flux. This is not due to an orientation effect, the warp directly impacts the observed distribution of fluxes, with the southern cone being much brighter than its northern counterpart. This

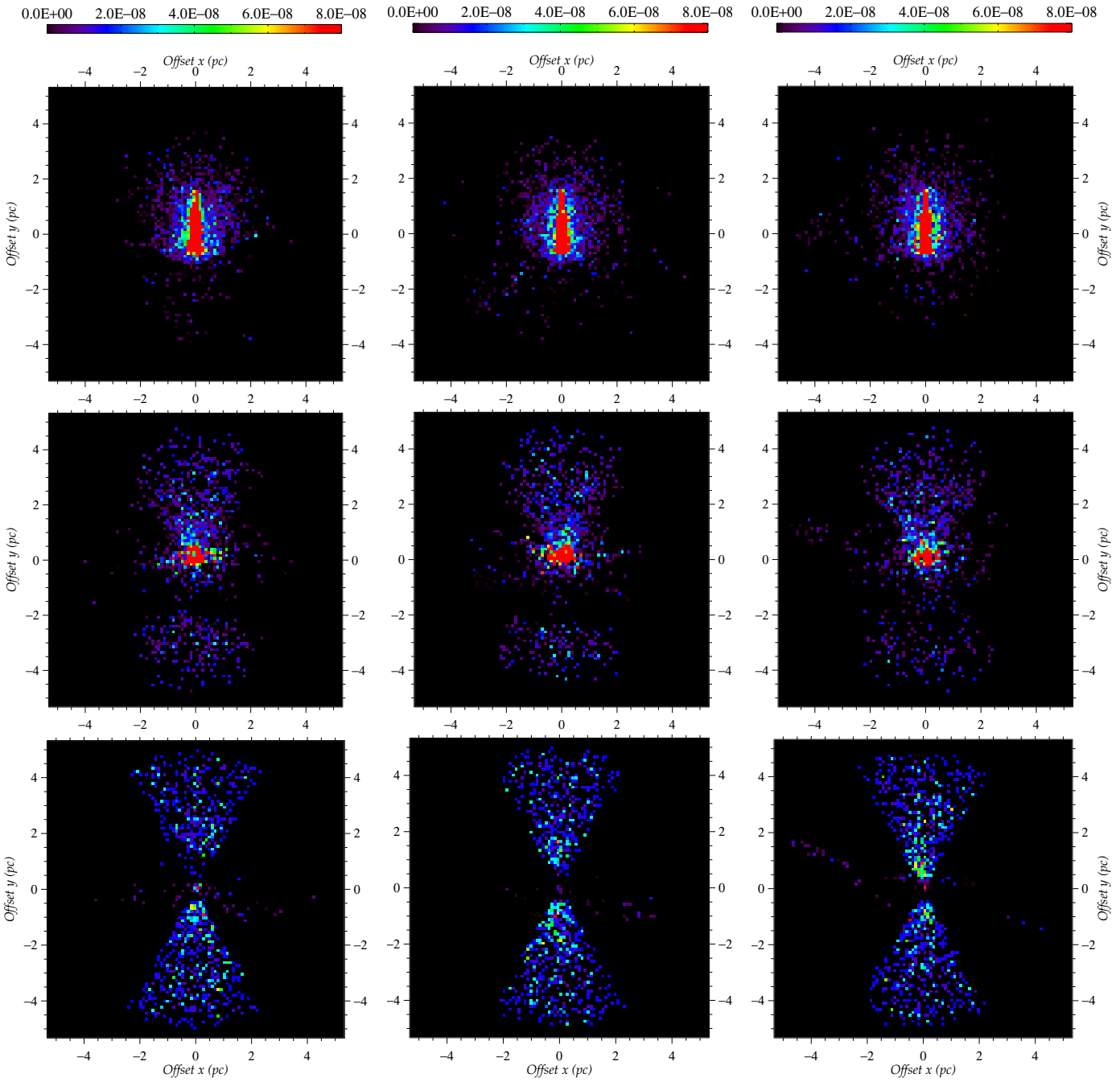

Fig. 9. Polarized flux maps of a complex AGN model using a warped and clumpy dusty torus with $R_{\rm warp}$ = 2 pc and $\theta_{\rm warp}$ = 30°, such as in Fig. 1. The polarized flux is color coded (in arbitrary units, but identically scaled for all panels). The axes are in parsecs. The *first row* shows a nucleus orientation of 18°, the *second row* an inclination of 50° and the *last row* 87°. Each column shows a different azimuthal angle: 0°, 45°, and 90°.

naturally explains why most of the variations in P and PPA observed in Figs. 7 and 8 occurs at an azimuthal angle of 0°. Rotating the AGN slowly uncovers the northern wind base and equilibrates the distribution of polarized fluxes. When the maximum asymmetry of the model is reached (azimuthal angle 90°), the upper and lower warps can both be detected thanks to multiple scattering, but their relative importance is too weak to impact the integrated polarization properties (see the low polarization fractions on Fig. 10). The ratio between the polar scattered flux and the flux from the warped torus surfaces tells us that warped tori might be difficult to detect even with current polarimetric observatories.

5. Exploring the warp morphology

We shown that warped dusty tori are acceptable within the unified model picture as long as they do not violate one of the most important rules of the paradigm: there must be a polarization dichotomy between Seyfert-I and Seyfert-II orientations. Owing to the clumpiness of the circumnuclear structure and the parametrization of the warps, a limited number of exceptions can arise, but the majority of the models have proven to pass the test when adding additional AGN components. Yet, the question of the importance of the warp morphology remains because the method for producing warps is not unique. To illustrate how a similar model can change the resulting polarization degree and

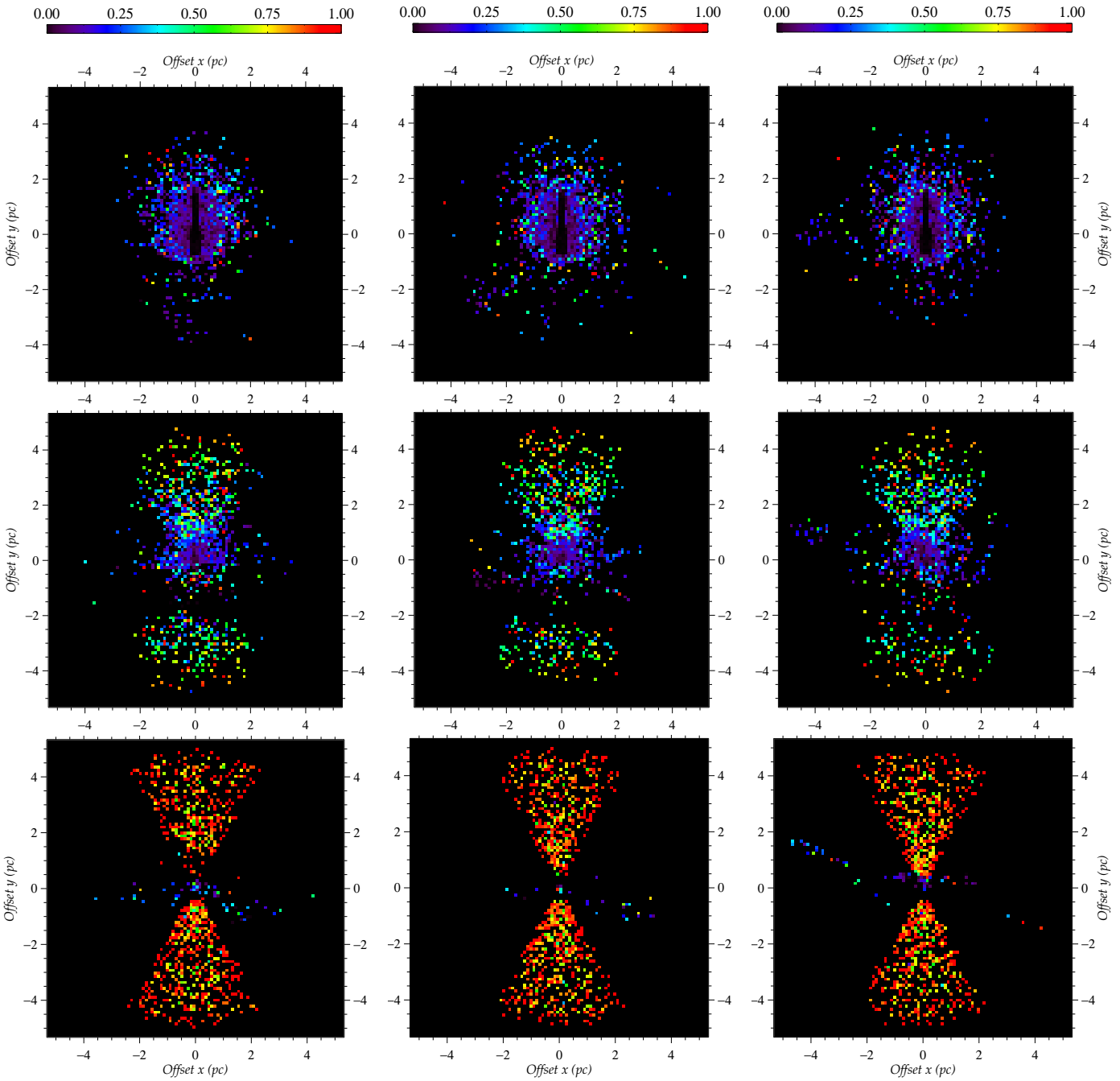

Fig. 10. Same as Fig. 9 but showing the optical polarization fraction ranging from 0 (unpolarized) to 1 (fully polarized).

angle, we took the dust distribution from Jud et al. (2017) and implemented it into STOKES. We clumped the structure such that its volume-filling factor was the same as in the models investigated so far. A sketch of the corresponding smooth-density distribution model is shown in Fig. 12.

Running our Monte Carlo code for an isolated, warped, and clumpy dusty torus, we found several similarities and differences with respect to the baseline model presented in this paper. In Fig. 13, we present the polarization results for the Jud model (left-hand side panels, in red) and for a warped torus (right-hand side panels, in black) created with the formulas presented in this paper. We used $R_{\rm warp} = 0.5$ pc and $\theta_{\rm warp} = 10°$ to be as close as possible to the former structure. It appears that the model from Jud et al. (2017) produces different amounts of polarization degree associated with sharp sawtooth variations of the PPA when the observer is revolving around the structure. The polarization angle modulations occur at the same azimuthal angle, with minor variations due to the random distribution of clumps. However, the polarization degree in Jud models is always superior to 0.1%, while in the case of the warped tori discussed in the previous sections of this paper, P was often lower than 0.1%. The sharp diminution in P associated with the PPA rotations are not seen here due to the puffed-up structure of the warped component that enhances the scattering probabilities. This peculiarity could be used to constrain the geometry of warped tori around point sources[3]. In the cases of the intermediate and equatorial

[3] Such as warps in protoplanetary and dusty debris disks (Heap et al. 2000; Schneider et al. 2014; Marino et al. 2015).

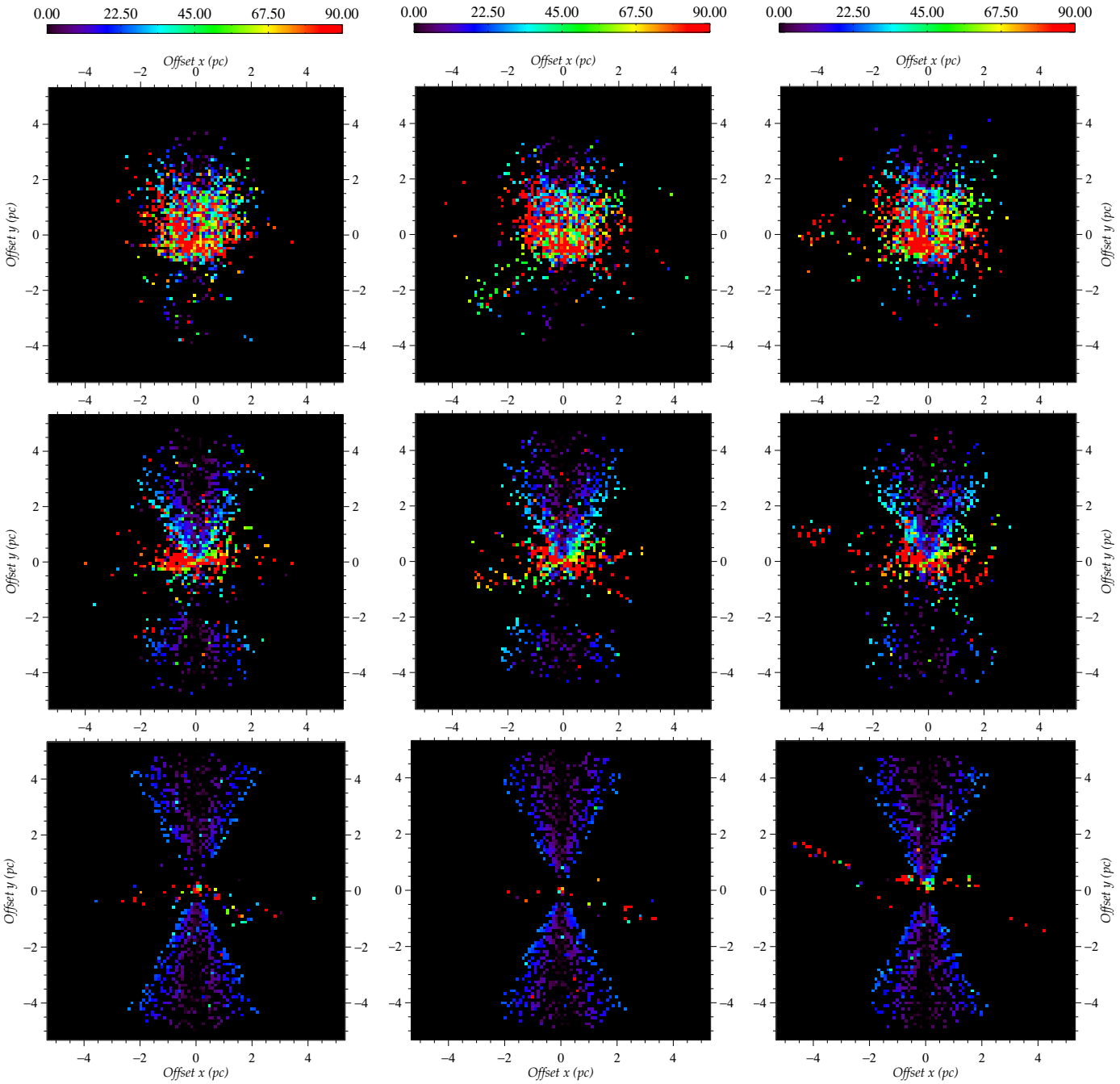

Fig. 11. Same as Fig. 9 but showing the optical polarization position angle ranging from 0° (perpendicular polarization angle with respect to the projected radio axis of the system) to 90° (parallel polarization angle).

viewing angles, the observer's line-of-sight passes through the bulk of the obscuring material, but the deep PPA polarization modulations still occur. Compared to the models of this paper, the geometry of the warped disk from Jud et al. (2017) presents high and rapid variations of the polarization degree and no stabilization of the polarization angle around 0°.

Including the other two components (equatorial radiation-supported disk and ionization cones) in the warped torus allowed us to check the polarization properties of a hypothetical AGN with a Jud dusty disk (Fig. 14, left-hand side panels, in red) compared to our warped toy-model (Fig. 14, right-hand side panels, in black). The properties of the additional components are the same as before, therefore differences in the AGN polarization

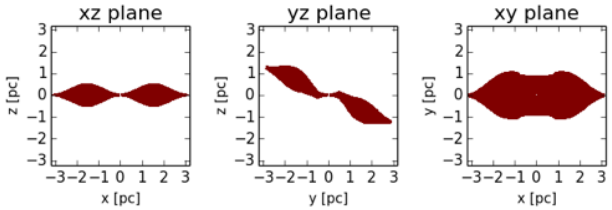

Fig. 12. Cuts through the dust density distribution of the standard model shown in Jud et al. (2017), taken along the coordinate planes. The model was clumpy and then implemented in STOKES.

signatures will reflect the impact of the warped structure. The most striking result of Fig. 14 is that the model violates the

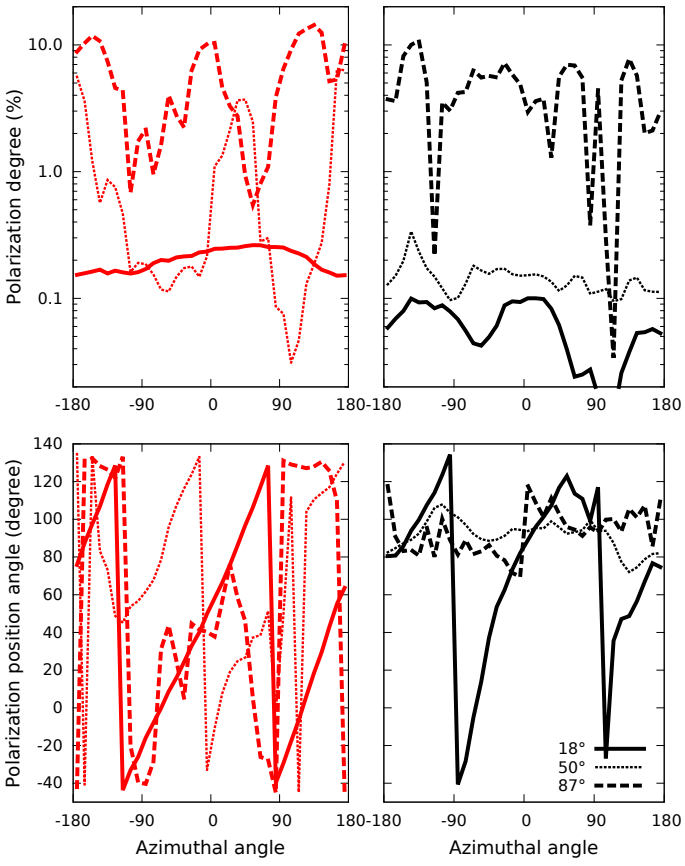

Fig. 13. *Left panels*: optical polarization (5000 Å) from the warped dusty disk presented in Jud et al. (2017). For comparison, a warped torus created with the formulas presented in this paper using $R_{\rm warp}$ = 0.5 pc and $\theta_{\rm warp}$ = 10° is shown (black, *right panels*). The parametrization of Jud's disk is the same as in their paper and the model was clumpy in order to achieve a 22–23% volume-filling factor.

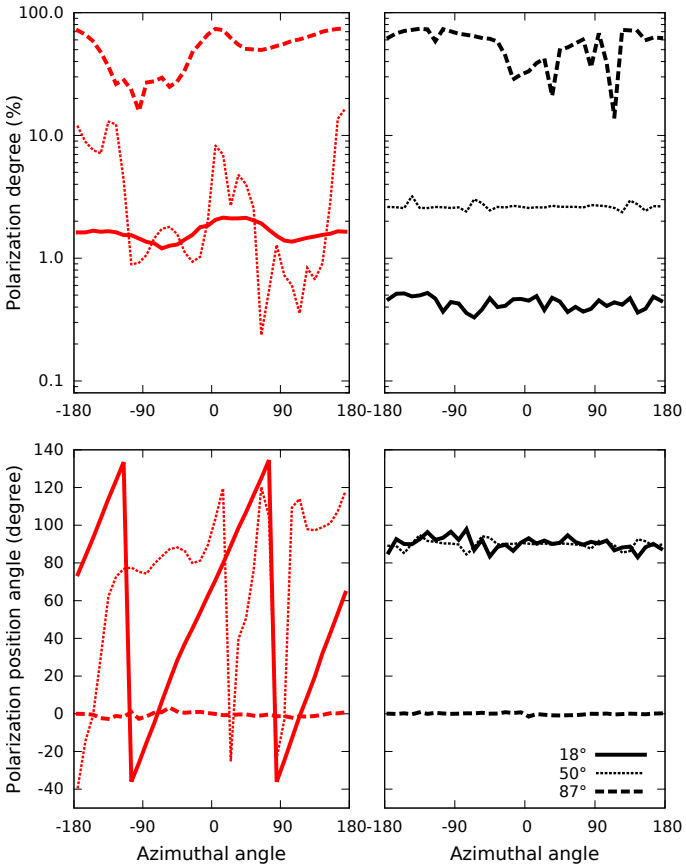

Fig. 14. Same as Fig. 13, with the addition of a radiation-supported disk and polar outflows. The final models are thus similar to the AGN prescription studied in Sect. 4.

predictions from the unified model: for face-on and intermediate inclinations, the polarization position angle is neither parallel nor perpendicular to the projected polar axis of the system, but has preserved its sawtooth oscillations despite the additional scattering components. The difference is due to the geometry of the torus: 1) the model from Jud et al. (2017) has a concave shape (e.g., a sphere cut out), whereas the warped torus model from this paper has a convex shape in the innermost region (an elliptical cross section, Goosmann & Gaskell 2007); and 2) the width of the warped dusty medium from Jud et al. (2017), extending toward the polar region, is twice as large as in the model from this paper. The change in morphology enhances the scattering probabilities for the Jud model and more scattered radiation bounces from the dust structure beyond $R_{\rm warp}$ to a polar observer. The polarization signatures from the warped torus are preserved and result in variable PPA. Together with the degree of polarization (1 to 2%), this is unfortunately in contradiction to observations. These high degrees of P are rare among Seyfert-Is and are most of the time associated with a perpendicular polarization angle (the so-called polar-scattering dominated AGN, see Smith et al. 2002; and Marin 2016). According to this model, all pole-on AGN should present high degrees of polarization together with an apparent random distribution of PPA. The case is similar for intermediate inclinations, but it is more aligned with the prediction of the AGN paradigm. Intermediate orientations are allowed to produce $P > 1\%$, and the simulation shows that the polarization angle reaches a plateau at 0° or 90° according to the phase. For edge-on inclinations, the model is dominated by scattering inside the electron cone and is in agreement with polarimetric expectations of Seyferts (P = 20–80% and perpendicular polarization angle, see Marin 2014).

6. Outlook

We presented an optical investigation of the continuum polarization from warped tori. The time and resources required by the simulations to run polarized transfer in a clumpy medium are high enough to explain why such work was never undertaken previously. With the development of faster codes, a more complete view of the polarimetric signature of warped and clumpy media is in reach, especially extending the wavelength range of our work. In particular, two codes are perfectly suited in the infrared band. SKIRT, presented in Baes et al. (2003, 2011) and Camps & Baes (2015), is a radiative transfer code that simulates the journey of photon packages in dusty astrophysical systems. Thanks to an adaptive grid, SKIRT handles any three-dimensional geometry of the dust distribution and offers a full treatment of multiple anisotropic scattering, absorbing, and (re-)emitting media, which makes it a perfect tool to extend the work accomplished in this paper. The polarization of radiation by spherical dust grains is included and should soon be released to the public (Peest et al. 2017). The second infrared tool, MontAGN, is dedicated to the production of high angular resolution polarization maps (Grosset et al. 2017). The code shares many common points with STOKES and also includes re-emission by dust, computing temperature equilibrium adjustment at each absorp-

tion. MontAGN works by sending photon packets that travel in a user-defined grid of dusty cells, such as SKIRT, and overlaps the wavelengths band of STOKES in the 0.8–1 μm regime. This allowed for a comparison between the codes (Grosset et al. 2016; Marin et al. 2016b), which gave satisfactory results. The use of a grid in both infrared codes makes the creation of a clumpy medium easy and computationally cheap. It might become easier to check whether a defined warped configuration can explain the observed infrared polarization of nearby Seyferts, which is intrinsically less polluted by starlight emission than in the optical band. The importance of re-emission and multiple scattering, depolarizing the escaping radiation, will probably be enhanced by clumpiness and may lead to different signatures in PPA than in the V and B bands.

Another waveband of importance is the X-ray band. With the advance of modern polarimeters, either based on the photoelectric effect (e.g., Costa et al. 2001), gas-filled time-projection chambers (e.g., Black et al. 2007), or Compton scattering (e.g., Guo et al. 2013), it will soon be possible to measure the X-ray polarization from nearby and bright AGN. The expected AGN polarization in the soft energy band (2–10 keV) should be of similar levels than in the optical band (Marin et al. 2016a), but due to Compton and inverse-Compton scattering, the hard X-ray band might show a distinctive polarization. It is thus important to produce new simulations of AGN including clumpy tori based on contemporary observations (Marinucci et al. 2016). Preliminary results for smooth-density warped disks were recently obtained by Cheng et al. (2016), who computed the X-ray polarimetric features induced by a warped disk around a stellar-mass black hole. Using the Bardeen-Petterson effect, the authors explored the possibility of identifying a warped disk with X-ray spectropolarimetric measurements of the thermal spectrum of the accretion disk. Among other findings, they showed that the warped structure can be identified by a transition in polarization in the 0.1–3 keV band. The higher the inclination between the inner and outer part of the warped accretion disk, the more prominent the feature. By looking from a polar direction, it might be possible to detect this feature with a future mission, but the surrounding of the accreting system must be taken into account first (polar outflows being among the most important regions to add). The detection of an X-ray polarization signal influenced by a warped accreting medium might even be enhanced by Lense-Thirring precession of the inner accretion flow. Ingram et al. (2015) found that the polarization signature emitted from a truncated disk/precessing inner flow geometry in an X-ray binary oscillates at a specific frequency where quasi-periodic oscillations are detected. The maximum polarization degree due to the Lense-Thirring effect is on the order of 1.5%, which is not negligible for a potential detection. The case for AGN remains to be explored, but encouraging results are emerging for the detection and characterization of warped structures around compact objects.

7. Conclusions

We explored the optical scattering-induced continuum polarization emerging from clumpy and warped dusty tori. Significant features appear at Seyfert-I inclinations, where the polarization position angle rotates by ~180° in sawtooth oscillations, locally decreasing the degree of polarization. At intermediate and edge-on inclinations, both P and the PPA are similar to non-warped clumpy tori. Examining a wide range of warp parameters, we found that the impact of clumpiness onto P overwhelms the signatures of warps, and it is almost impossible to distinguish between two different warped structures.

By including a warped torus in a more complex AGN model, with equatorial inflows and polar outflows, we were able to recover the observed polarization properties of nearby Seyferts, together with a proper distinction in polarization angles between a Seyfert-I and a Seyfert-II. This indicates that warped equatorial structures may exist in AGN, leaving very little imprints on the optical continuum. However, imaging polarimetry is able to reveal the warps in Seyfert-IIs, but the sensitivity, contrast, and angular resolution needed to achieve a detection are beyond current observatories, despite the progresses made by direct-imaging instruments equipped with extreme adaptive optics systems (Gratadour et al. 2015).

If warped equatorial tori may indeed exist in AGN and pass the polarimetric tests of the unified model, the exact geometry of the warped structure must be examined carefully. We have proven that not all geometries are able to reproduce the observed polarization dichotomy. In this case, any new model of dusty disk-born winds (Czerny & Hryniewicz 2011), warped disks (Lawrence & Elvis 2010), or exotic self-gravitating tori (Trova et al. 2016) must be investigated using polarimetry. Polarized radiative transfer simulations will then ensure that the structure is consistent with the most geometry-sensitive tool the unified model has to offer.

Acknowledgements. The authors would like to acknowledge the anonymous referee for useful comments that improved the quality of the paper. The authors are also grateful to D. Gratadour and L. Grosset from LESIA; M. Stalevski from the University of Chile; R. W. Goosmann and B. Vollmer from the Observatory of Strasbourg; K. Tristram from the European Southern Observatory, L. Burtscher from the faculty of Sterrewacht Leiden; and R. Antonucci from the University of California for useful discussions and comments that greatly helped to ameliorate this manuscript.

References

Antonucci, R. 1993, ARA&A, 31, 473
Antonucci, R. R. J. 1984, ApJ, 278, 499
Antonucci, R. R. J., & Miller, J. S. 1985, ApJ, 297, 621
Asmus, D., Hönig, S. F., & Gandhi, P. 2016, ApJ, 822, 109
Augereau, J. C., Nelson, R. P., Lagrange, A. M., Papaloizou, J. C. B., & Mouillet, D. 2001, A&A, 370, 447
Baes, M., Davies, J. I., Dejonghe, H., et al. 2003, MNRAS, 343, 1081
Baes, M., Verstappen, J., De Looze, I., et al. 2011, ApJS, 196, 22
Bardeen, J. M., & Petterson, J. A. 1975, ApJ, 195, L65
Black, J. K., Baker, R. G., Deines-Jones, P., Hill, J. E., & Jahoda, K. 2007, Nucl. Instrum. Methods, 581, 755
Bock, J. J., Neugebauer, G., Matthews, K., et al. 2000, AJ, 120, 2904
Burtscher, L., Jaffe, W., Raban, D., et al. 2009, ApJ, 705, L53
Burtscher, L., Meisenheimer, K., Tristram, K. R. W., et al. 2013, A&A, 558, A149
Camps, P., & Baes, M. 2015, Astronomy and Computing, 9, 20
Caproni, A., & Abraham, Z. 2004, ApJ, 602, 625
Capetti, A., Macchetto, F., Axon, D. J., Sparks, W. B., & Boksenberg, A. 1995, ApJ, 452, L87
Capetti, A., Axon, D. J., Macchetto, F., Sparks, W. B., & Boksenberg, A. 1996, ApJ, 466, 169
Caproni, A., Mosquera Cuesta, H. J., & Abraham, Z. 2004, ApJ, 616, L99
Cheng, Y., Liu, D., Nampalliwar, S., & Bambi, C. 2016, Class. Quant. Grav., 33, 125015
Costa, E., Soffitta, P., Bellazzini, R., et al. 2001, Nature, 411, 662
Czerny, B., & Hryniewicz, K. 2011, A&A, 525, L8
Gallimore, J. F., Baum, S. A., & O'Dea, C. P. 2004, ApJ, 613, 794
Gallimore, J. F., Elitzur, M., Maiolino, R., et al. 2016, ApJ, 829, L7
García-Burillo, S., Combes, F., Ramos Almeida, C., et al. 2016, ApJ, 823, L12
Gillessen, S., Perrin, G., Brandner, W., et al. 2006, in SPIE Conf. Ser., Proc. SPIE, 6268, 626811
Goosmann, R. W., & Gaskell, C. M. 2007, A&A, 465, 129
Gratadour, D., Rouan, D., Grosset, L., Boccaletti, A., & Clénet, Y. 2015, A&A, 581, L8

Grosset, L., Marin, F., Gratadour, D., et al. 2016, SF2A-2016: Proc. Annual Meeting of the French Society of Astronomy and Astrophysics, 57
Grosset, L., Rouan, D., Gratadour, D., et al. 2017, A&A, submitted
Gunn, J. E. 1979, in Active Galactic Nuclei (Cambridge University Press), 213
Guo, Q., Beilicke, M., Garson, A., et al. 2013, Astropart. Phys., 41, 63
Hao, L., Weedman, D. W., Spoon, H. W. W., et al. 2007, ApJ, 655, L77
Heap, S. R., Lindler, D. J., Lanz, T. M., et al. 2000, ApJ, 539, 435
Herrnstein, J. R., Moran, J. M., Greenhill, L. J., et al. 1999, Nature, 400, 539
Hönig, S. F., Beckert, T., Ohnaka, K., & Weigelt, G. 2006, A&A, 452, 459
Ingram, A., Maccarone, T. J., Poutanen, J., & Krawczynski, H. 2015, ApJ, 807, 53
Jaffe, W., Meisenheimer, K., Röttgering, H. J. A., et al. 2004, Nature, 429, 47
Jud, H., Schartmann, M., Mould, J., Burtscher, L., & Tristram, K. R. W. 2017, MNRAS, 465, 248
Kartje, J. F. 1995, ApJ, 452, 565
Kishimoto, M., Antonucci, R., Cimatti, A., et al. 2001, ApJ, 547, 667
Kishimoto, M., Hönig, S. F., Beckert, T., & Weigelt, G. 2007, A&A, 476, 713
Kishimoto, M., Hönig, S. F., Antonucci, R., et al. 2009a, A&A, 507, L57
Kishimoto, M., Hönig, S. F., Tristram, K. R. W., & Weigelt, G. 2009b, A&A, 493, L57
Kiuchi, K., Sekiguchi, Y., Kyutoku, K., et al. 2015, Phys. Rev. D, 92, 064034
Kollmeier, J. A., Onken, C. A., Kochanek, C. S., et al. 2006, ApJ, 648, 128
Krolik, J. H., & Begelman, M. C. 1988, ApJ, 329, 702
Lawrence, A., & Elvis, M. 2010, ApJ, 714, 561
López-Gonzaga, N., Burtscher, L., Tristram, K. R. W., Meisenheimer, K., & Schartmann, M. 2016, A&A, 591, A47
Maiolino, R., Risaliti, G., Salvati, M., et al. 2010, A&A, 517, A47
Manske, V., Henning, T., & Men'shchikov, A. B. 1998, A&A, 331, 52
Marin, F. 2014, MNRAS, 441, 551
Marin, F. 2016, MNRAS, 460, 3679
Marin, F., & Antonucci, R. 2016, ApJ, 830, 82
Marin, F., & Goosmann, R. W. 2014, in SF2A-2014: Proc. of the Annual Meeting of the French Society of Astronomy and Astrophysics, eds. J. Ballet, F. Martins, F. Bournaud, R. Monier, & C. Reylé, 103
Marin, F., & Stalevski, M. 2015, in SF2A-2015: Proc. of the Annual Meeting of the French Society of Astronomy and Astrophysics, eds. F. Martins, S. Boissier, V. Buat, L. Cambrésy, & P. Petit, 167
Marin, F., Goosmann, R. W., Gaskell, C. M., Porquet, D., & Dovčiak, M. 2012, A&A, 548, A121
Marin, F., Goosmann, R. W., & Gaskell, C. M. 2015, A&A, 577, A66
Marin, F., Goosmann, R. W., & Petrucci, P.-O. 2016a, A&A, 591, A23
Marin, F., Grosset, L., Goosmann, R., et al. 2016b, SF2A-2016: Proc. of the Annual Meeting of the French Society of Astronomy and Astrophysics, 103
Marino, S., Perez, S., & Casassus, S. 2015, ApJ, 798, L44
Marinucci, A., Bianchi, S., Matt, G., et al. 2016, MNRAS, 456, L94
Mason, R. E., Levenson, N. A., Shi, Y., et al. 2009, ApJ, 693, L136
Mathis, J. S., Rumpl, W., & Nordsieck, K. H. 1977, ApJ, 217, 425
Menou, K., & Quataert, E. 2001, ApJ, 552, 204
Meyer, F. 1989, Theory of accretion disks, NATO Advanced Science Institutes (ASI) Series C, 290
Miller, J. S., Goodrich, R. W., & Mathews, W. G. 1991, ApJ, 378, 47
Nayakshin, S. 2005, MNRAS, 359, 545
Nenkova, M., Ivezić, Ž., & Elitzur, M. 2002, ApJ, 570, L9
Nenkova, M., Sirocky, M. M., Ivezić, Ž., & Elitzur, M. 2008a, ApJ, 685, 147
Nenkova, M., Sirocky, M. M., Nikutta, R., Ivezić, Ž., & Elitzur, M. 2008b, ApJ, 685, 160
Netzer, H. 2013, The Physics and Evolution of Active Galactic Nuclei (Cambridge, UK: Cambridge University Press)
Nikutta, R., Elitzur, M., & Lacy, M. 2009, ApJ, 707, 1550
Peest, C., Camps, P., Stalevski, M., Baes, M., & Siebenmorgen, R. 2017, A&A, 601, A92
Phinney, E. S. 1989, in NATO Advanced Science Institutes (ASI) Series C, ed. F. Meyer, 290, 457
Pier, E. A., & Krolik, J. H. 1992, ApJ, 401, 99
Prevot, M. L., Lequeux, J., Prevot, L., Maurice, E., & Rocca-Volmerange, B. 1984, A&A, 132, 389
Pringle, J. E. 1996, MNRAS, 281, 357
Sazonov, S., Churazov, E., & Krivonos, R. 2015, MNRAS, 454, 1202
Schartmann, M., Meisenheimer, K., Camenzind, M., et al. 2008, A&A, 482, 67
Schneider, G., Grady, C. A., Hines, D. C., et al. 2014, AJ, 148, 59
Schnorr-Müller, A., Davies, R. I., Korista, K. T., et al. 2016, MNRAS, 462, 3570
Shuder, J. M. 1981, ApJ, 244, 12
Siebenmorgen, R., Heymann, F., & Efstathiou, A. 2015, A&A, 583, A120
Smith, J. E., Young, S., Robinson, A., et al. 2002, MNRAS, 335, 773
Stalevski, M., Fritz, J., Baes, M., Nakos, T., & Popović, L. Č. 2012, MNRAS, 420, 2756
Stokes, G. G. 1851, Transactions of the Cambridge Philosophical Society, 9, 399
Sturm, E., Hasinger, G., Lehmann, I., et al. 2006, ApJ, 642, 81
Swain, M., Vasisht, G., Akeson, R., et al. 2003, ApJ, 596, L163
Tristram, K. R. W., Meisenheimer, K., Jaffe, W., et al. 2007, A&A, 474, 837
Tristram, K. R. W., Burtscher, L., Jaffe, W., et al. 2014, A&A, 563, A82
Trova, A., Karas, V., Slaný, P., & Kovář, J. 2016, ApJS, 226, 12
Urry, C. M., & Padovani, P. 1995, PASP, 107, 803
Wada, K., Schartmann, M., & Meijerink, R. 2016, ApJ, 828, L19
Wolf, S., & Henning, T. 1999, A&A, 341, 675
Young, S. 2000, MNRAS, 312, 567